ACS APPLIED MATERIALS & INTERFACES

Research Article

www.acsami.org

Coating Lithium Titanate with Nitrogen-Doped Carbon by Simple Refluxing for High-Power Lithium-Ion Batteries

Du Hoang Long,[†,§] Min-Gi Jeong,[†] Yoon-Sung Lee,[†] Wonchang Choi,[†,§] Joong Kee Lee,[†,§] In-Hwan Oh,[†,§] and Hun-Gi Jung*[,†,§]

[†]Center for Energy Convergence, Green City Technology Institute, Korea Institute of Science and Technology, Hwarangno 14 gil 5, Seongbuk-gu, Seoul 136-791, Republic of Korea

[§]Department of Energy and Environmental Engineering, Korea University of Science and Technology, 176 Gajungro, Yuseong-gu, Daejeon 305-350, Republic of Korea

Supporting Information

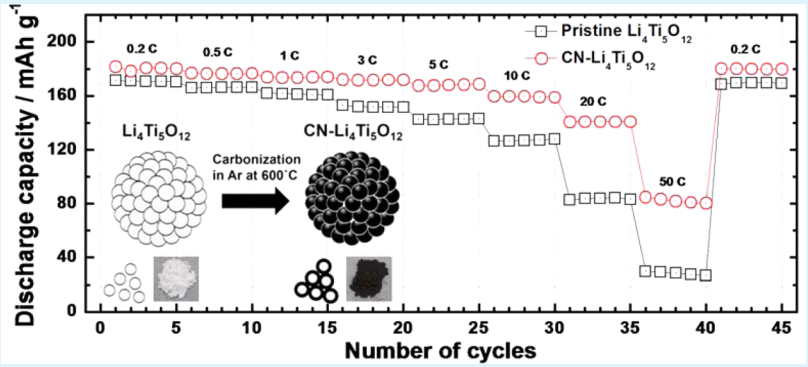

ABSTRACT: Nitrogen-doped carbon is coated on lithium titanate ($Li_4Ti_5O_{12}$, LTO) via a simple chemical refluxing process, using ethylenediamine (EDA) as the carbon and nitrogen source. The process incorporates a carbon coating doped with a relatively high amount of nitrogen to form a conducting network on the LTO matrix. The introduction of N dopants in the carbon matrix leads to a higher density of C vacancies, resulting in improved lithium-ion diffusion. The uniform coating of nitrogen-doped carbon on $Li_4Ti_5O_{12}$ (CN-LTO) enhances the electronic conductivity of a CN-LTO electrode and the corresponding electrochemical properties of the cell employing the electrode. The results of our study demonstrate that the CN-LTO anode exhibits higher rate capability and cycling performance over 100 cycles. From the electrochemical tests performed, the specific capacity of CN-LTO electrode at higher rates of 20 and 50 C are found to be 140.7 and 82.3 mAh g^{-1}, respectively. In addition, the CN-$Li_4Ti_5O_{12}$ anode attained higher capacity retention of 100% at 1 C rate after 100 cycles and 92.9% at 10 C rate after 300 cycles.

KEYWORDS: *lithium titanate, nitrogen-doped carbon coating, anode, lithium ion battery, high power density*

INTRODUCTION

Lithium-ion batteries (LIBs) are widely used in many portable electronic devices because of their high energy and power densities.[1] However, the rate performance of LIBs must be further improved for application in large-scale energy-storage devices such as electrical vehicles (EVs),[2−4] which require fast charge and discharge rates to decrease the time required for charging to about 2 h for the current generation of EVs. Therefore, in addition to investigating advanced nanostructured electrode materials that are capable of improving the rate performance of LIBs, it is imperative that these materials also exhibit enhanced kinetics of solid-state diffusion of Li^+ ions during intercalation and deintercalation, as well as high values of electronic conductivity.

Recently, extensive research has been dedicated to lithium titanante ($Li_4Ti_5O_{12}$, LTO) spinel as a promising anode material for LIBs. Compared with commercial graphite-based anode materials, LTO exhibits a flat and relatively high lithium insertion−extraction potential plateau at approximately 1.55 V (vs Li/Li^+). As most of the organic electrolytes are stable at this potential, the formation of a solid−electrolyte interface (SEI) layer and the safety problems associated with dendritic lithium formation can be avoided. Moreover, because of its negligible volume change upon lithiation and delithiation, LTO demonstrates excellent cycling stability. Lithiation in LTO is a two-phase system, which allows fast Li^+ ions cooperative motion, thereby avoiding Li plating at high C rates.[5−8] Therefore, these intrinsic advantages of LTO contribute to the stability and safety of LIBs and would enable them to fulfill the requirements for application in EVs.[9,10] However, LTO

Received: January 26, 2015
Accepted: April 29, 2015
Published: April 29, 2015

DOI: 10.1021/acsami.5b00776
ACS Appl. Mater. Interfaces 2015, 7, 10250−10257

possesses insulating properties originating from the empty Ti 3d states with a band gap energy of 2 eV, as well as a moderate lithium-ion diffusion rate (D_{Li^+}) of 2×10^{-8} cm^2 s^{-1}, which results in poor rate capability of the LTO-based cells. This is one of the main factors hindering commercial applications of the material.[11−13] To date, various strategies have been adopted to optimize the rate performance of LTO, and the most commonly used methods are reducing the particle size,[14−16] doping with supervalent cations,[17−19] and coating the LTO surface with conductive materials.[20,21] Reducing the particle size shortens the Li^+-diffusion pathway and increases the electrochemical active area between the electrolyte and the electrode, which is expected to improving the rate capability of the electrode material. Doping with supervalent cations decreases the area-specific impedance (ASI) of the LTO electrode and increases the rate capability. Coating the LTO surface with conductive materials, such as carbon, provides a continuous electron pathway from the outer to inner part of the LTO particle and thus improves the electron conductivity; the conductive coating can also be permeable for Li^+ ions from the surrounding electrolyte solution. Among these approaches, the coating method is the simplest and most convenient way for commercially available LIBs because it preserves the physical properties of pristine LTO, such as the morphology, particle size, and powder tap density.[20,21]

In our previous study, we reported that a carbon coating on LTO anode material improved the electronic conductivity and subsequently enhanced the electrochemical performance of the cell.[10,20] Furthermore, a carbon coating can effectively improve the electrochemical performance of the electrode when nitrogen is introduced in the carbon structure as a dopant.[22] The nitrogen-doped-carbon-coated active material is believed to further improve the electronic conductivity, Li^+-ion diffusion through the carbon layers, and the charge transfer at the interface, which contribute significantly toward a good reversible capacity and an enhanced rate capability of the anode.[23,24] The electronic conductivity is increased by the formation of metallic conductive TiN between the active material and the coating, which causes reduction of Ti^{4+} to a more conductive Ti^{3+} phase. The facilitation of Li^+-ion permeability is ascribed to defects in the carbon matrix caused by the existence of nitrogen dopants.

In this work, we developed a simple coating technique using ethylenediamine (EDA) as a carbon and nitrogen source to form a thin layer of nitrogen-doped carbon on the surface of LTO (CN-LTO) nanoparticles, which was aggregated to form micrometer-sized spherical secondary particles. We demonstrated that the as-obtained spherical CN-LTO exhibited significant improvements in electronic conductivity and electrochemical performance when used as an anode material for LIBs.

EXPERIMENTAL SECTION

Synthesis of Pristine and Nitrogen-Doped-Carbon-Coated LTO Materials. The two-step synthetic process used to prepare CN-LTO is schematically illustrated in Scheme 1. In the first step, the spherical LTO powder was synthesized using a spray-drying process followed by solid-state calcination, as previously reported.[25] The precursor materials containing LiOH (Sigma-Aldrich), anatase TiO_2 nanoparticles (Sigma-Aldrich), and a polyvinylpyrrolidone (Sigma-Aldrich) as dispersant (5 wt %, relative to TiO_2) were dissolved and dispersed in distilled water and the molar ratio of lithium to titanium was 4:5. The prepared precursor slurries were mixed with zirconia balls by a planetary mill at a speed of 300 rpm for 12 h. The homogeneously mixed slurries were atomized by a two-fluid nozzle at a pressure of 3 kg cm^{-2} at 250 °C. The collected, spray-dried precursor powder was further calcined at 900 °C for 20 h in air to obtain pristine LTO.

Scheme 1. Schematic Diagram of Nitrogen-Doped-Carbon Coating Process

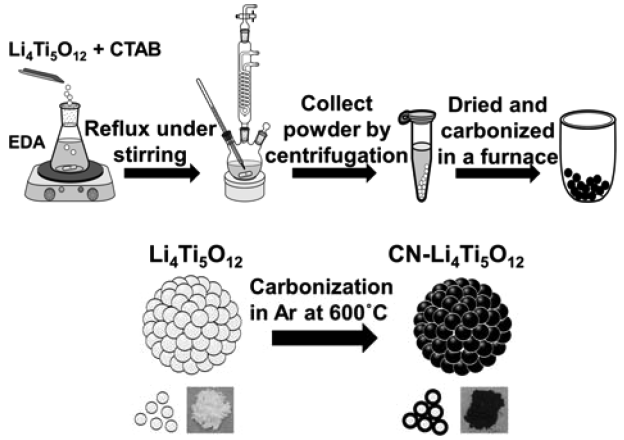

In the second step, 1 g of as-prepared pristine LTO and 0.5 g of cetyltrimethylammonium bromide (CTAB) (Sigma-Aldrich) were dispersed in 100 mL of an EDA solution (Sigma-Aldrich) with continuous stirring and refluxing at 120 °C for 48 h. After this step, the precipitate (LTO covered by EDA) was obtained by centrifugation at 7000 rpm and dried in an oven overnight. Finally, the obtained powder was calcined for 4 h at 600 °C in a furnace purged with Ar gas.

Characterization of Synthesized Materials. The morphologies of the resulting samples were examined using a field-emission scanning electron microscope (FE-SEM; S-4200, Hitachi, Japan). The crystalline structures of the synthesized materials were characterized by powder X-ray diffraction (XRD; Rigaku D/MAX-2500 V/PC, Japan) measurements, using Cu K_α radiation to obtain diffraction data in the 2θ range of 10−80°. The amounts of doped carbon and nitrogen in the synthesized materials were determined by an elemental analyzer (EA1108/CHNS-0, Carlo Erba/Fisons/CE Instrument, Milan, Italy). A four-point probe (CMT-SR2000N, AIT Co., Korea) was employed for the direct volt−ampere method to measure the electrical conductivity of disc-shaped pellets of the final products. To prepare disc-shaped pellets of LTO and CN-LTO, measured amount of powders were respectively put in one round-shaped die body above one round-shaped die base. A piston was thereupon inserted to press the powders into pellets. Two pellets of both LTO and CN-LTO must have similar thickness such as 2 mm due to accuracy. In addition, the presence of carbon coatings and the reaction of nitrogen with other elements in either the coating or the active material were observed through a high-resolution transmission electron microscope (HR-TEM; JEM-2010, JEOL, Japan) and an X-ray photoelectron spectroscope (XPS; PHI 5000 VersaProbe, Ulvac-PHI, Japan), respectively. An Al K_α X-ray monochromator ($h\nu$ = 1486.6 eV; 25 W; 15 kV anode) was used as a source in the spectroscope and the XPS was calibrated against a binding energy of 284.6 eV (C 1s peak).

The electrochemical performances were evaluated using CR2032 coin-type cells. The LTO electrode was prepared by mixing 80 wt % active material (pristine and CN-LTO), 10 wt % carbon black conducting agent (acetylene black), and 10 wt % polyvinylidene fluoride (PVdF) binder with *N*-methyl-2-pyrrolidone (NMP) solution to form a slurry, which was then pasted on the copper-foil current collector. Li metal foil was used as the counter electrode and the electrolyte was 1.2 M $LiPF_6$ solution in ethylene carbonate−diethyl carbonate (EC−DEC, volume ratio of 1:1) absorbed in a porous polyethylene separator (Celgard). The electrodes were assembled in the CR2032 coin-type cells with the electrolyte and the separator, and it was performed inside a dry glovebox filled with argon gas. The cells were used for further electrochemical characterization.

DOI: 10.1021/acsami.5b00776
ACS Appl. Mater. Interfaces 2015, 7, 10250−10257

The galvanostatic measurements were carried out using a battery testing system (Series 4000, Maccor, USA). The cells were cycled at room temperature (25 °C), high temperature (60 °C) by channels located in a heated oven, and low temperature (−10 and −20 °C) by channels located in a refrigerator, with a potential window between 1.0 and 3.0 V. The electrochemical performances of the cells were measured at various current densities: 35 (0.2 C rate), 87.5 (0.5 C rate), 175 (1 C rate), 525 (3 C rate), 875 (5 C rate), 1750 (10 C rate), 3500 (20 C rate), and 8750 mA g^{-1} (50 C rate).

RESULTS AND DISCUSSION

Figure 1 shows the XRD patterns of the synthesized pristine LTO and CN-LTO samples. All the peaks in both patterns

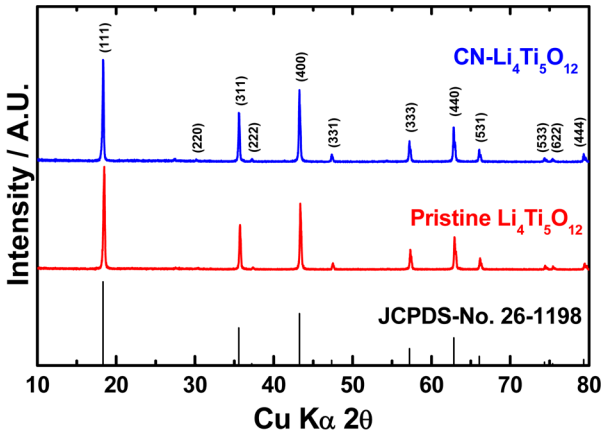

Figure 1. X-ray diffraction patterns of the synthesized pristine $Li_4Ti_5O_{12}$ and CN-$Li_4Ti_5O_{12}$ samples.

correspond to the standard $Li_4Ti_5O_{12}$ spinel (JCPDS card no. 26-1198), which confirms that the EDA used for nitrogen-doped-carbon coating did not affect the pristine LTO's cubic phase with *Fd*3*m* space group. The pattern of CN-LTO also confirms the characteristic pure cubic spinel structure, with no evidence of impurity phases. As shown in Table 1, which summarizes the physical properties of synthesized samples, the cubic lattice parameters *a* of pristine LTO and CN-LTO were calculated by the least-squares method to be 8.345 and 8.359 Å, respectively, which agree well with values obtained in previous studies.[5−21] The lattice parameter of CN-LTO was slightly larger than that for the pristine sample, which was expected if some of the Ti^{4+} with smaller ionic radius (0.605 Å) were transformed to Ti^{3+} with larger ionic radius (0.67 Å).[20] In addition, the XRD pattern of CN-LTO reveals that its carbon constituent was amorphous in nature, with no discernible diffraction features.

The morphologies of the synthesized samples were observed using the SEM and HR-TEM, as shown in Figure 2. The size of the secondary spherical particles comprising ∼100 nm primary particles was found to be 5 μm in Figure 2a. The presence of nanometer-sized particles is believed to reduce the Li^+-ion-diffusion pathways and could therefore improve the kinetics of lithium-ion intercalation into the LTO host structure. In

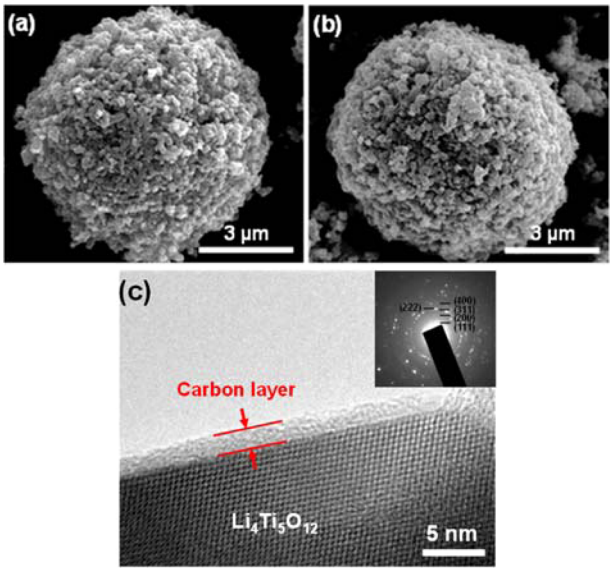

Figure 2. SEM images of (a) pristine $Li_4Ti_5O_{12}$ and (b) CN-$Li_4Ti_5O_{12}$ samples. (c) High-resolution TEM image of CN-$Li_4Ti_5O_{12}$ after calcination at 600 °C.

addition, the agglomeration of primary nanoparticles into a micrometer-sized secondary particle shows that the tap density of the resulting electrodes was higher than that of LTO nanoparticles. As shown in Figure 2b, the spherical morphology and microstructures were maintained even after nitrogen-doped carbon from the EDA precursor was coated on LTO at a high temperature. In addition, the high-resolution TEM image in Figure 2c shows that the doped carbon layer with a thickness of 2 nm was uniformly coated on the surface of the primary particles. This carbon layer offered a few advantages. First, when compared with pristine LTO, the carbon-coated powder was protected from the corrosive environment at the interface between LTO and the electrolyte during long cycling. Second, the electrons could find a simple conduction pathway through the carbon layer. Third, the thin outer carbon layer with randomly distributed defects and vacancies could facilitate the Li^+ ions' migration to the LTO particle surface. Thus, this balance between the electronic and ionic transport led to improved electrochemical performance of the $Li_4Ti_5O_{12}$ electrode, which would be beneficial for the enhanced power densities of lithium-ion batteries.[26] The selected-area electron diffraction (SAED) pattern, as shown in the inset of Figure 2c, also confirms the crystallinity of the LTO phase, which is in good agreement with the properties estimated from XRD analysis.

We carried out XPS analysis to investigate the properties of the carbon coating on $Li_4Ti_5O_{12}$. The XP spectra of the pristine LTO and CN-LTO are shown in Figure 3a, where the peaks correspond to O 1s, N 1s, Ti 2p, and C 1s. In contrast to the pristine LTO sample, the spectrum of CN-LTO clearly shows a new peak centered at 399 eV (Figures 3a and b), which can be

Table 1. Physical Properties of Pristine $Li_4Ti_5O_{12}$ and CN-$Li_4Ti_5O_{12}$

					lattice parameters	
sample	carbon content (wt %)	nitrogen content (wt %)	electronic conductivity (S cm^{-1})	tap density (g cm^{-3})	*a* (Å)	volume (Å^3)
$Li_4Ti_5O_{12}$			1.58×10^{-9}	1.062	8.345(7)	581.290
CN-$Li_4Ti_5O_{12}$	5.9	1.7	4.29×10^{-6}	1.416	8.359(5)	584.185

DOI: 10.1021/acsami.5b00776
ACS Appl. Mater. Interfaces 2015, 7, 10250−10257

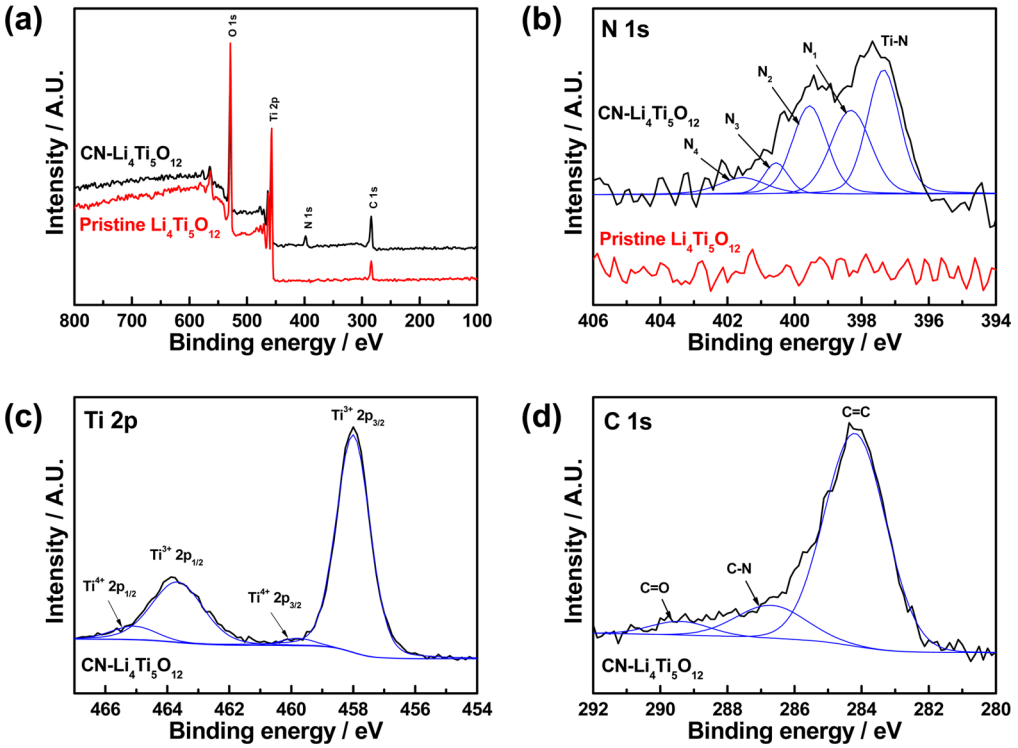

Figure 3. (a) X-ray photoelectron (XP) spectra of pristine $Li_4Ti_5O_{12}$ and CN-$Li_4Ti_5O_{12}$. High-resolution XP spectra showing the (b) N 1s, (c) Ti 2p, and (d) C 1s peaks of pristine $Li_4Ti_5O_{12}$ and CN-$Li_4Ti_5O_{12}$.

attributed to the N 1s peak, indicating the presence of nitrogen in the carbon coating. As shown in Figure 3b, the high-resolution XP spectrum of N 1s for CN-LTO sample can be deconvolved into five peaks, indicating the presence of multiple states of N. The peaks with binding energies of 398.3, 399.5, 400.5, and 401.5 eV can be attributed to pyridinic (N_1), pyrrolic (N_2), graphitic (N_3), and oxide of pyridinic (N_4) nitrogen, respectively.[27−29] More specifically, N_1 represents the pyridinic configuration of nitrogen (C═N−C), originating from N atoms with two sp^2 hybridized C neighbors, where the N atom replaces a carbon atom in the C_6 ring. N_2 is pyrrolic nitrogen in a C_5 ring and donates two electrons to the system.[30] The pyridinic and pyrrolic N are located at the edge of the graphite sheets and are known as vacancy generators in the carbon matrix, which would enhance Li-ion diffusion.

As shown in Scheme 2, pyridinic N, with a valence electron pair in a nonbonding sp^2 orbital, did not participate in the conjugated bond system, whereas the pyridinic N atom played a role as a p-type dopant and was able to create C vacancies in the carbon layer. The large adsorption energies of the Li^+ ions at the pyridinic and pyrrolic defects with low energy barrier for lithium penetration guaranteed the high rate capability for lithium intercalation and deintercalation. The graphitic N (or quaternary N) with three sp^2 carbon neighbors is represented by the N_3 peak. The graphitic N atom was located in the graphitic carbon plane where it replaced a carbon atom and had two of the valence electrons occupying the p_z orbital of nitrogen. Hence, the nitrogen atoms could be ionized and liberated electrons could contribute to the system (compared to one electron per carbon atom). The excess electrons could produce the "-doping" effect. Therefore, the graphitic N accounted for the increase in electronic conductivity.[31−33] In summary, these three states of nitrogen have equal benefits on the battery performance instead of owning individual one.

Scheme 2. Schematic Representation of Nitrogen-Doped Carbon

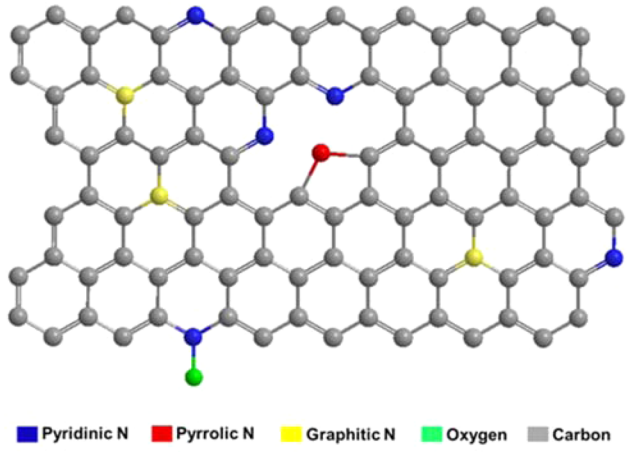

Consequently, these have to be balanced so that the material can satisfy criteria of high electronic conductivity and high ionic diffusion for battery applications.

Furthermore, a peak was observed at 397.3 eV, which is close to the binding energy of TiN (397.0 eV) reported in the literature,[34] and the slight shift was caused by the formation of a Ti−N−C-like compound.[35] To reveal the bonding nature of nitrogen to titanium in TiN, the nitrogen atom was assumed to be an electron donor in the carbon plane and would thus increase the electron-donating ability to the titanium atom. By trapping electrons from the nitrogen atom, the titanium atom would have the tendency to reduce Ti^{4+} cations to the Ti^{3+} state,[36] which would increase the electronic conductivity. In addition, the reduction of Ti^{4+} to Ti^{3+} was confirmed by peaks of the Ti 2p spectrum in Figure 3c. The binding energies of

DOI: 10.1021/acsami.5b00776
ACS Appl. Mater. Interfaces 2015, 7, 10250−10257

Ti^{3+} $2p_{3/2}$ and Ti^{3+} $2p_{1/2}$ correspond to the peak positions at 457.9 and 463.6 eV, respectively, which are similar to previously reported values.[37] The presence of Ti^{3+} in the structure appeared to have directly affected the lattice parameter so that the coated LTO had a larger lattice parameter than the pristine LTO sample, as indicated by the values in Table 1. Nevertheless, the presence of nitrogen in the carbon layer is confirmed by the XP spectrum of C 1s in Figure 3d, with the 186.7 eV peak corresponding to the presence of the C−N bond.[38]

Table 1 also shows the physicochemical properties of the pristine LTO and CN-LTO samples. As determined by elemental analysis, the mass ratios of carbon and nitrogen in the CN-LTO sample were 5.9 and 1.7 wt %, respectively. The electronic conductivities of pristine LTO and CN-LTO were found to be 1.58×10^{-9} and 4.29×10^{-6} S cm^{-1}, respectively. With increased electronic conductivity, the nitrogen-doped carbon layer could improve the transportation of electrons between LTO and the current collector, as confirmed by the high rate with high density in the electrochemical performances. The CN-LTO exhibited a significantly higher tap density of 1.416 g cm^{-3}, which is ascribed to the tighter packing of the secondary particles.

The lattice parameters of the pristine and coated LTO samples are important indicators of the effects of either carbon coating or nitrogen-doped-carbon coating on the cell performance because the valence state of Ti could be estimated. As shown in Table 1, the lattice parameters of CN-LTO (a = 8.359(5) Å, V = 584,185 $Å^3$) were larger than those of pristine LTO (a = 8.345(7) Å, V = 581.290 $Å^3$). We believe that the carbon coating source, EDA, and the strong reduction atmosphere (Ar) during calcination both contributed to the partial transformation of the initial Ti^{4+} to Ti^{3+}. The increase in lattice parameter was related to the presence of Ti^{3+}, formed by the reduction of Ti^{4+} to Ti^{3+}, because the radius of Ti^{3+} is larger than that of Ti^{4+}. In addition, electrons that hopped from Ti^{4+} to Ti^{3+} created oxygen vacancies; therefore, more oxygen vacancies meant more Ti^{3+} were present, leading to an increase in the lattice parameters.[39] Furthermore, the reduction of Ti sites, which was induced by oxygen-vacancy generation in LTO, could improve the electronic conductivity of the samples, as reported in previous studies,[40] although there were also serious drawbacks. First of all, the conductivity was gradually degraded over time because in the oxygen vacancy site, Ti^{3+} was readily reoxidized into the original Ti^{4+} by accepting an electron from O^{2-} in air, which mostly affected the cyclic performance of the electrode.[41,42] Second, the oxygen-vacancy generation could lead to distortion of the LTO lattice, thereby decreasing the Li^+ diffusion.[43] However, in the case of CN-LTO, the reduction process of the Ti^{4+} cations was possibly facilitated by accepting the electrons of the nitrogen atom in the carbon matrix, as suggested in the analysis of the TiN peak in the XP spectrum, which would have partially overcome the issues of oxygen vacancy. Indeed, the electrochemical performances clearly demonstrate the effects of nitrogen in the layer.

To further investigate the effects of nitrogen-doped-carbon coating and trivalent Ti, we performed cell tests with anodes composed of the as-synthesized LTO samples. The initial charge and discharge curves are shown in Figure 4 for the cells with pristine and CN-LTO anodes at the same charge and discharge current densities ranging from 0.2 (35 mA g^{-1}) to 50 C rate (8,500 mA g^{-1}) between 1.0 and 3.0 V. The pristine LTO cell delivered a discharge capacity of 161.2 mAh g^{-1} at 1

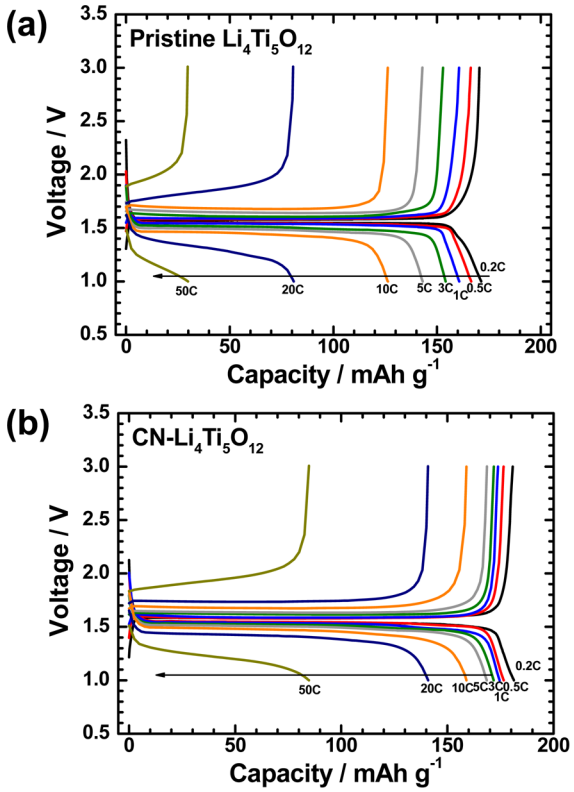

Figure 4. Charge−discharge curves of pristine (a) $Li_4Ti_5O_{12}$ and (b) CN-$Li_4Ti_5O_{12}$ at various current densities from 0.2 to 50 C rate. The charging rates were the same as the discharging rates.

C rate, while the CN-LTO cell achieved a higher discharge capacity of 173.8 mAh g^{-1} at the same rate, which is very close to the theoretical capacity of LTO (175 mAh g^{-1}). At low current densities from 0.2 to 1 C rate, both cells with and without nitrogen-doped-carbon coating showed a flat operating potential plateau of 1.55 V (vs Li/Li^+), which is attributed to the redox reaction of Ti^{3+}/Ti^{4+}.[25] However, at higher current densities from 5 to 50 C rate, the potential plateau of both cells became shorter and showed a relatively high overpotential profile. The discharge capacities gradually decreased as the current density increased, thereby demonstrating polarization and slowing of the reaction kinetics.[38] A comparison of the two samples showed that the pristine LTO exhibited relatively higher degree of polarization and lower reaction kinetics than CN-LTO at a higher current density, which is caused by the more electrically conductive nitrogen-doped-carbon coating on the CN-LTO surface, the mixed valence state change of Ti (coexistence of trivalent and tetravalent Ti), and the improved electrochemical performance of CN-LTO. The Coulombic efficiency of the cells had a constant value of about 100%, indicating that the Li^+ intercalation and deintercaltion of the synthesized LTO samples were completely reversible even at extremely high currents.

The discharge capacities of the cells with pristine LTO and CN-LTO anodes at various discharge and charge rates between 0.2 (35 mA g^{-1}) and 50 C rate (8750 mA g^{-1}) were sustained for 5 cycles at each setting, as shown in in Figure 5. The discharge capacities of the CN-LTO cell were higher than those of the pristine LTO cell at all tested current densities. At 20 C rate, the rate capability of CN-LTO was higher with a capacity retention of 78.0%, compared with the capacity retention of

DOI: 10.1021/acsami.5b00776
ACS Appl. Mater. Interfaces 2015, 7, 10250−10257

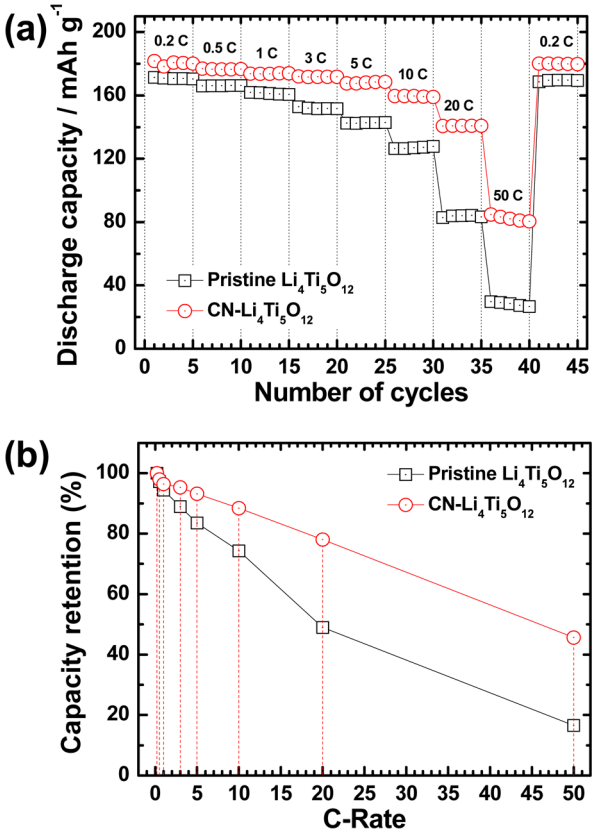

Figure 5. (a) Rate capability and (b) capacity retention of pristine $Li_4Ti_5O_{12}$ and CN-$Li_4Ti_5O_{12}$ electrodes at C rates between 0.2 and 50 C. The charging rates were the same as the discharging rates.

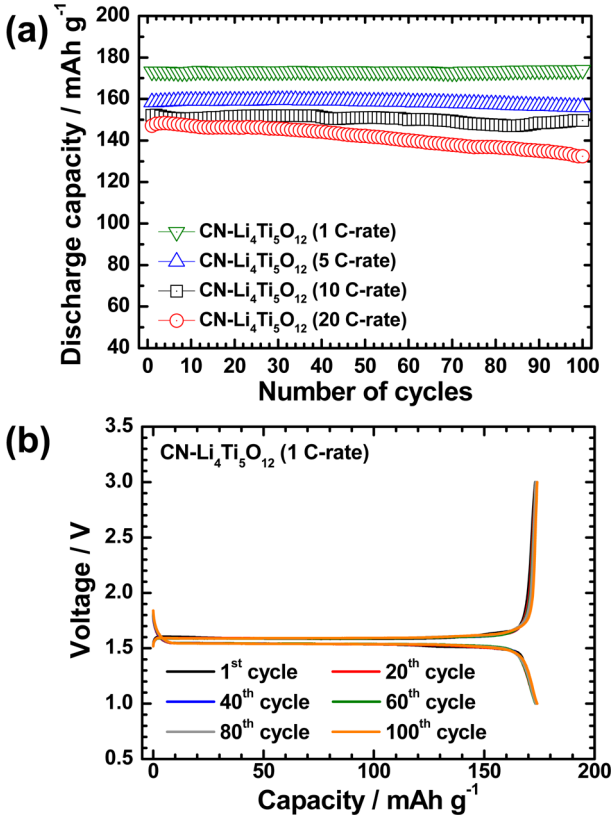

Figure 6. (a) Cycling performance of CN-$Li_4Ti_5O_{12}$ at rates varying from 1 to 20 C. (b) Charge−discharge curves of CN-$Li_4Ti_5O_{12}$ between various cycles at 1 C rate (b). The charging rates were the same as the discharging rates.

only 48.9% for the pristine LTO cell. The enhanced performance of the CN-LTO electrode is attributed to the characteristics of the nitrogen-doped-carbon coating on LTO. Moreover, even at a current rate as high as 50 C rate, the CN-LTO cell delivered the excellent discharge capacity of 82.3 mAh g^{-1} while the pristine LTO could only deliver 28.3 mAh g^{-1}.

The electrochemical properties of the nitrogen-doped-carbon-coated LTO anode was carried out under the harshest conditions of cycling at high current density (Figure 6) and in a wide operating temperature range (Figure 7). Figure 6a shows the capacity retention of the CN-LTO cells at 1, 5, 10, and 20 C rate over 100 cycles. The capacity retentions after 100 cycles at 1, 5, 10, and 20 C rate were 100, 98.5, 98.4, and 90.0%, respectively, at room temperature. As shown in Figure 6b, the capacity and curves at the initial and final cycles remained at about 100% with stable and low polarization. To obtain better evidence of the effects of nitrogen-doped-carbon-coated LTO on the electrochemical performance, a comparison of the cycling performance of the cells with pristine LTO and CN-LTO anodes was evaluated at 10 C rate for 300 cycles. As shown in Figure S1 in Supporting Information, the CN-LTO cell showed a capacity retention of 92.9% after 300 cycles, while the pristine LTO showed a gradual drop in capacity with a capacity retention of only 54.3% after 300 cycles.

The performance of the coated LTO samples was evaluated over a temperature range of −20 to +60 °C. Being able to maintain high performance at extreme temperatures is required for the efficient operation of energy-storage devices such as storage of renewable energy, as well as the powering of electric car engines. Figure 7a shows that the cells completely satisfied this requirement with a very stable capacity delivery even at these extreme temperature limits, with a capacity retention of 95.4% after 100 cycles at −20 °C. It also showed a higher discharge capacity at 60 °C, than at room temperature, which could be attributed to the enhanced kinetics of Li^+-ion diffusion. In addition, the initial charge−discharge curves at 1 C rate (Figure 7b) showed lower polarization than at room temperature. These results indicate that CN-LTO with enhanced electronic conductivity would be a promising anode material for high-performance lithium-ion batteries with high energy and power density.

CONCLUSIONS

We synthesized CN-LTO powder with a simple chemical refluxing process, using EDA as the carbon and nitrogen source and CTAB as a surfactant. The CN-LTO cell exhibited excellent discharge capacities of 173.8, 153.6, and 140.8 mAh g^{-1} at 1, 10, and 20 C rate, respectively. CN-LTO showed complete cycle stability, with negligible capacity fading over 100 cycles at 1 C rate and 92.9% of capacity retention at 10 C rate after 300 cycles. This impressive electrochemical performance of the CN-LTO anode is attributed to (i) the effect of uniformly coated conductive carbon to provide an easy pathway for electrons, (ii) the effect of graphitic N and pyridinic N in donating extra electrons for increasing electronic conductivity, and (iii) the appearance of the reduction of Ti^{4+} to more a conductive phase, Ti^{3+}. We suggest that this new approach of nitrogen-doped-carbon coating can be applied to design various

DOI: 10.1021/acsami.5b00776
ACS Appl. Mater. Interfaces 2015, 7, 10250−10257

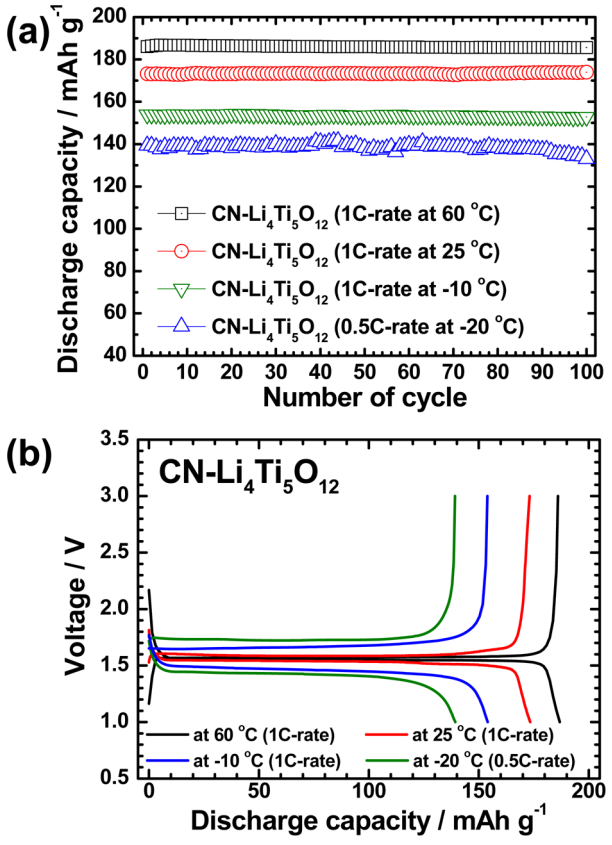

Figure 7. (a) Cycling performance and (b) voltage profiles of the initial cycles of CN-$Li_4Ti_5O_{12}$ in a temperature range from −20 to 60 °C.

electrode materials for high-energy and high-power density batteries for hybrid and electric vehicles.

■ ASSOCIATED CONTENT

Supporting Information

Additional results of electrochemical performances of nitrogen-doped-carbon-coated $Li_4Ti_5O_{12}$. The Supporting Information is available free of charge on the ACS Publications website at DOI: 10.1021/acsami.5b00776.

■ AUTHOR INFORMATION

Corresponding Author

*E-mail: hungi@kist.re.kr.

Notes

The authors declare no competing financial interest.

■ ACKNOWLEDGMENTS

This work was supported by the National Research Foundation of Korea Grant funded by the Korean Government (MEST) (NRF-2010-C1AAA001-2010-0028958) and by the KIST institutional program.

■ REFERENCES

(1) Hsiao, K. C.; Liao, S. C.; Chen, J. M. Microstructure Effect on the Electrochemical Property of $Li_4Ti_5O_{12}$ as an Anode Material for Lithium-Ion Batteries. *Electrochim. Acta* **2008**, *53*, 7242−7247.

(2) Guo, X. F.; Wang, C. Y.; Chen, M. M.; Wang, J. Z.; Zheng, J. M. Carbon Coating of $Li_4Ti_5O_{12}$ Using Amphiphilic Carbonaceous Material for Improvement of Lithium-Ion Battery Performance. *J. Power Sources* **2012**, *214*, 107−112.

(3) Yoshio, M.; Wang, H.; Fukuda, K.; Hara, Y.; Adachi, Y. Effect of Carbon Coating on Electrochemical Performance of Treated Natural Graphite as Lithium-Ion Battery Anode Material. *J. Electrochem. Soc.* **2000**, *147*, 1245−1250.

(4) Scrosati, B.; Hassoun, J.; Sun, Y.-K. Lithium-Ion Batteries: A Look into the Future. *Energy Environ. Sci.* **2011**, *4*, 3287−3295.

(5) Colbow, K. M.; Dahn, J. R.; Haering, R. R. Structure and Electrochemistry of the Spinel Oxides $LiTi_2O_4$ and $Li_{4/3}Ti_{5/3}O_4$. *J. Power Sources* **1989**, *26*, 397−402.

(6) Ohzuku, T.; Ueda, A.; Yamamoto, N. Zero-Strain Insertion Material of $Li[Li_{1/3}Ti_{5/3}]O_4$ for Rechargeable Lithium Cells. *J. Electrochem. Soc.* **1995**, *142*, 1431−1435.

(7) Ronci, F.; Reale, P.; Scrosati, B.; Panero, P.; Rossi Albertini, V.; Perfetti, P.; di Michiel, M.; Merino, J. M. High-Resolution In-Situ Structure Measurements of the $Li_{4/3}Ti_{5/3}O_4$ "Zero-Strain" Insertion Material. *J. Phys. Chem. B* **2002**, *106*, 3082−3086.

(8) Zaghib, K.; Mauger, A.; Groult, H.; Goodenough, J. B.; Julien, C. M. Advanced Electrodes for High Power Li-Ion Batteries. *Materials* **2013**, *6*, 1028−1049.

(9) Takami, N.; Inagaki, H.; Kishi, T.; Harada, Y.; Fujita, Y.; Hoshina, K. Electrochemical Kinetics and Safety of 2-V Class Li-Ion Battery System Using Lithium Titanium Oxide Anode. *J. Electrochem. Soc.* **2009**, *156*, A128−A132.

(10) Jung, H.-G.; Jang, M. W.; Hassoun, J.; Sun, Y.-K.; Scrosati, B. A High-Rate Long-Life $Li_4Ti_5O_{12}$/$Li[Ni_{0.45}Co_{0.2}Mn_{1.45}]O_4$ Lithium-Ion Battery. *Nat. Commun.* **2011**, *2*, 516 DOI: 10.1038/ncomms1527.

(11) Ouyang, C. Y.; Zhong, Z. Y.; Lei, M. S. Ab Initio Studies of Structural and Electronic Properties of $Li_4Ti_5O_{12}$ Spinel. *Electrochem. Commun.* **2007**, *9*, 1107−1112.

(12) Brousse, T.; Fragnaud, P.; Marchand, R.; Schleich, D. M.; Bohnke, O.; West, K. All Oxide Solid-State Lithium-Ion Cells. *J. Power Sources* **1997**, *68*, 412−415.

(13) Zaghib, K.; Simoneau, M.; Armand, M.; Gauthier, M. Electrochemical Study of $Li_4Ti_5O_{12}$ as Negative Electrode for Li-Ion Polymer Rechargeable Batteries. *J. Power Sources* **1999**, *81*−*82*, 300−305.

(14) Borghols, W. J. H.; Wagemaker, M.; Lafont, U.; Kelder, E. M.; Mulder, F. M. Size Effects in the $Li_{4+x}Ti_5O_{12}$ Spinel. *J. Am. Chem. Soc.* **2009**, *131*, 17786−17792.

(15) Kavan, L.; Grätzel, M. Facile Synthesis of Nanocrystalline $Li_4Ti_5O_{12}$ (Spinel) Exhibiting Fast Li Insertion. *Electrochem. Solid-State Lett.* **2002**, *5*, A39−A42.

(16) Junrong, L.; Zilong, T.; Zhongtai, Z. Controllable Formation and Electrochemical Properties of One-Dimentional Nanostructured Spinel $Li_4Ti_5O_{12}$. *Electrochem. Commun.* **2005**, *7*, 894−899.

(17) Ohzuku, T.; Tatsumi, K.; Matoba, N.; Sawai, K. Electrochemistry and Structure Chemistry of $Li[CrTi]O_4$ (*Fd*3*m*) in Nonaqueous Lithium Cells. *J. Electrochem. Soc.* **2000**, *147*, 3592−3597.

(18) Sun, Y.-K.; Jung, D.-J.; Lee, Y.-S.; Nahm, K. S. Synthesis and Elctrochemical Characterization of Spinel $Li[Li_{(1-x)/3}Cr_xTi_{(5-2x)/3}]_4$ Anode Materials. *J. Power Sources* **2004**, *125*, 242−245.

(19) Huang, S.; Wen, Z.; Zhu, X.; Lin, Z. Effects of Dopant on the Electrochemical Performance of $Li_4Ti_5O_{12}$ as Electrode Material for Lithium Ion Batteries. *J. Power Sources* **2007**, *165*, 408−412.

(20) Jung, H.-G.; Myung, S.-T.; Yoon, C. S.; Son, S.-B.; Oh, K. H.; Amine, K.; Scrosati, B.; Sun, Y.-K. Microscale Spherical Carbon-Coated $Li_4Ti_5O_{12}$ as Ultra High Power Anode Material for Lithium Batteries. *Energy Environ. Sci.* **2011**, *4*, 1345−1351.

(21) Li, H.; Zhou, H. Enhancing the Performances of Li-Ion Batteries by Carbon-Coating: Present and Future. *Chem. Commun.* **2012**, *48*, 1201−1217.

(22) Paraknowitsch, J. P.; Thomas, A.; Antonietti, M. A Detailed View on the Polycondensation of Ionic Liquid Monomers towards Nitrogen Doped Carbon Materials. *J. Mater. Chem.* **2010**, *20*, 6746−6758.

(23) Zhao, L.; Hu, Y.-S.; Li, H.; Wang, Z.; Chen, L. Porous $Li_4Ti_5O_{12}$ Coated with N-Doped Carbon from Ionic Liquids for Li-Ion Batteries. *Adv. Mater.* **2011**, *23*, 1385−1388.

(24) Ming, H.; Ming, J.; Li, X.; Zhou, Q.; Wang, H.; Jin, L.; Fu, Y.; Zheng, J. Hierarchical $Li_4Ti_5O_{12}$ Particles Co-modified with C&N towards Enhanced Performance in Lithium-ion Battery Applications. *Electrochim. Acta* **2014**, *116*, 224−229.
(25) Jung, H.-G.; Kim, J.; Scrosati, B.; Sun, Y.-K. Micron-Sized, Carbon-Coated $Li_4Ti_5O_{12}$ as High Power Anode Material for Advanced Lithium Batteries. *J. Power Sources* **2011**, *196*, 7763−7766.
(26) Zhu, Z.; Cheng, F.; Chen, J. Investigation of Effects of Carbon Coating on the Electrochemical Performance of $Li_4Ti_5O_{12}$/C Nanocomposites. *J. Mater. Chem. A* **2013**, *1*, 9484−9490.
(27) Bhattacharyya, S.; Cardinaud, C.; Turban, G. Spectroscopic Determination of the Stucture of Amorphous Nitrogenated Carbon Films. *J. Appl. Phys.* **1998**, *83*, 4491−4500.
(28) Li, H.; Shen, L.; Yin, K.; Ji, J.; Wang, J.; Wang, X.; Zhang, X. Facile Synthesis of N-Doped Carbon-Coated $Li_4Ti_5O_{12}$ Microspheres Using Polydopamine as a Carbon Source for High Rate Lithium Ion Batteries. *J. Mater. Chem. A* **2013**, *1*, 7270−7276.
(29) Niwa, H.; Horiba, K.; Harada, Y.; Oshima, M.; Ikeda, T.; Terakura, K.; Ozaki, J.; Miyata, S. X-ray Absorption Analysis of Nitrogen Contribution to Oxygen Reduction Reaction in Carbon Alloy Cathode Catalysts for Polymer Electrolyte Fuel Cells. *J. Power Sources* **2009**, *187*, 93−97.
(30) Zheng, F.; Yang, Y.; Chen, Q. High Lithium Anodic Performance of Highly Nitrogen-Doped Porous Carbon Prepared from a Metal−Organic Framework. *Nat. Commun.* **2014**, *5*, 5261−5270.
(31) Mao, Y.; Duan, H.; Yu, B.; Zhang, L.; Hu, Y.; Zhao, C.; Wang, Z.; Chen, L.; Yang, Y. Lithium Storage in Nitrogen-Rich Mesoporous Carbon Materials. *Energy Environ. Sci.* **2012**, *5*, 7950−7955.
(32) Krstic, V.; Rikken, G. L. J. A.; Bernier, P.; Roth, S.; Glerup, M. Nitrogen Doping of Metallic Single-Walled Carbon Nanotubes: n-type Conduction and Dipole Scattering. *EPL* **2007**, DOI: 10.1209/0295-5075/77/37001.
(33) Luo, Z.; Lim, S.; Tian, Z.; Shang, J.; Lai, L.; MacDonald, B.; Fu, C.; Shen, Z.; Yu, T.; Lin, J. Pyridinic N Doped Graphene: Synthesis, Electronic Structure, and Electrocatalytic Property. *J. Mater. Chem.* **2011**, *21*, 8038−8044.
(34) Saha, N. C.; Tompkins, H. G. Titanium Nitride Oxidation Chemistry: An X-ray Photoelectron Spectroscopy Study. *J. Appl. Phys.* **1992**, *72*, 3072−3079.
(35) Zhao, L.; Hu, Y.-S.; Li, H.; Wang, Z.; Chen, L. Porous $Li_4Ti_5O_{12}$ Coated with N-Doped Carbon from Ionic Liquids for Li-Ion Batteries. *Adv. Mater.* **2011**, *23*, 1385−1388.
(36) Xiong, L.-B.; Li, J.-L.; Yang, B.; Yu, Y. Ti^{3+} in the Surface of Titanium Dioxide: Generation, Properties and Photocatalytic Application. *J. Nanomater.* **2012**, DOI: 10.1155/2012/831524.
(37) Hong, S. H.; Lee, J. Y.; Hong, S. J.; Cho, S. P.; Shin, C. H.; Hong, S. C.; Choi, S. H.; Kang, S. J.; Seo, P. W. Preparation Method of Vanadium/Titania-Based Catalyst Showing Excellent Nitrogen Oxide-Removal Performance at Wide Temperature Window Through Introduction of Ball Milling, and Use Thereof. U.S. Patent US 8088709 B2, Jan 12, 2012.
(38) Zhang, J.; Zhang, J.; Peng, Z.; Cai, W.; Yu, L.; Wu, Z.; Zhang, Z. Outstanding Rate Capability and Long Cycle Stability Induced by Homogeneous Distribution of Nitrogen Doped Carbon and Titanium Nitride on the Surface and in the Bulk of Spinel Lithium Titanate. *Electrochim. Acta* **2014**, *132*, 230−238.
(39) Wang, C.; Cheng, B. L.; Wang, S. Y.; Lu, H. B.; Zhou, Y. L.; Chen, Z. H.; Yang, G. Z. Effects of Oxygen Pressure on Lattice Parameter, Orientation, Surface Morphology and Deposition Rate of $(Ba_{0.02}Sr_{0.98})TiO_3$ Thin Films Grown on MgO Substrate by Pulsed Laser Deposition. *Thin Solid Films* **2005**, *485*, 82−89.
(40) Song, H.; Jeong, T.-G.; Moon, Y. H.; Chun, H.-H.; Chung, K. Y.; Kim, H. S.; Cho, B. W.; Kim, Y.-T. Stabilization of Oxygen-Deficient Structure for Conducting $Li_4Ti_5O_{12-\delta}$ by Mobybdenum Doping in a Reducing Atmosphere. *Sci. Rep.* **2014**, DOI: 10.1038/srep04350.
(41) Zuo, F.; Wang, L.; Wu, T.; Zhang, Z.; Borchardt, D.; Feng, P. Self-Doped Ti^{3+} Enhanced Photocatalyst for Hydrogen Production under Visible Light. *J. Am. Chem. Soc.* **2010**, *132*, 11856−11857.
(42) Komaguchi, K.; Maruoka, T.; Nakano, H.; Imae, I.; Ooyama, Y.; Harima, Y. Electron-Transfer Reaction of Oxygen Species on TiO_2 Nanoparticles Induced by Sub-band-gap Illumination. *J. Phys. Chem. C* **2009**, *114*, 1240−1245.
(43) Shin, J.-Y.; Joo, J. H.; Samuelis, D.; Maier, J. Oxygen-Deficient $TiO_{2-\delta}$ Nanoparticles via Hydrogen Reduction for High Rate Capability Lithium Batteries. *Chem. Mater.* **2011**, *24*, 543−551.

DOI: 10.1021/acsami.5b00776
ACS Appl. Mater. Interfaces 2015, 7, 10250−10257